# Advance In Micromechanics Analysis of Piezoelectric Composites

## Yi Xiao

Research School of Engineering, Australian National University, Acton, ACT 2601, Australia

## ABSTRACT

This paper presents an overview of micromechanics analysis of piezoelectric composites. Developments in micromechanics algorithms, finite element, and boundary element formulation for predicting effective material properties of piezoelectric composites are described. Finally, a brief summary of the approaches discussed is provided and future trends in this field are identified.

**Keywords:** Piezoelectric Composites, Micromechanics, Boundary Element

## I. INTRODUCTION

Piezoelectric material is such that when it is subjected to a mechanical load, it generates an electric charge. This effect is usually called the "piezoelectric effect". Conversely, when piezoelectric material is stressed electrically by a voltage, its dimensions change. This phenomenon is known as the "inverse piezoelectric effect". The study of piezoelectricity was initiated by J. and P. Curie in 1880 [1]. They found that certain crystalline materials generate an electric charge proportional to a mechanical stress. Since then new theories and applications of the field have been constantly advanced [2-10]. Voigt [2] developed the first complete and rigorous formulation of piezoelectricity in 1890. Since then several books on the phenomenon and theory of piezoelectricity have been written. Among them are the references by Cady [3], Tiersten [4], Parton and Kudryavtsev [5], Ikeda [6], Rogacheva [7], Qin [8-11], and Qin and Yang [12]. The first of these [2] treated the physical properties of piezoelectric crystals as well as their practical applications, the second [3] dealt with the linear equations of vibrations in piezoelectric materials, and the third and fourth [4, 5] gave a more detailed description of the physical properties of piezoelectricity. Rogacheva [7] presented general theories of piezoelectric shells. Qin [8-11] discussed Green's functions, advanced theory, and fracture mechanics of piezoelectric materials as well as applications to bone remodelling. Micromechanics of the piezoelectricity were discussed in [12]. These advances have resulted in a great number of publications including journal and conference papers. These include but not limit to applications to Branched crack problems[13-15], experimental investigation of bone materials [16-21], multi-field problems of bone remodelling [22-29], decay analysis of dissimilar laminates [30], moving crack problems [31], anti-plane crack problems [32, 33], fibre-pull out [34], fibre-push out [35-37], problems of frog Sartorius muscles [38], effective property evaluation [39-42], Green's function analysis [43-50], derivation of general solutions [51-55], boundary element analysis [56-63], micro-macro crack interaction problems [64], Trefftz finite element analysis [65-70], crack-inclusion problems [71, 72], crack growth problem [73, 74], multi-crack problems [75], crack-interface problems [76-78], closed crack-tip analysis [79], crack-path selection [80], penny-shaped crack analysis [81, 82], logarithmic singularity analysis [83], multi-layer piezoelectric actuator [84, 85], Symplectic mechanics analysis [86], fibre-reinforced composites [87], interlayer stress analysis [88], coupled thermo-electro-chemo-mechanical analysis [89], and damage analysis [90, 91].

Based on the analysis above, the present review consists of three major sections. Overall properties of three-dimensional (3D) are discussed in Section 2. Section 3 focuses on application of boundary element formulation to problems of piezoelectric materials for predicting effective material properties. Finally, a brief

summary on these sections is provided and areas that need further research are identified.

## II. METHODS AND MATERIAL

## I. Overall Properties of 3D Piezoelectric Composites

This section is concerned with the development an algorithm used in two-dimensional (2D) analysis for calculating transversely isotropic material properties. Since the finite element (FE) meshing patterns on the opposite areas are the same, constraint equations can be applied directly to generate appropriate load. The numerical results derived using this model have found a good agreement with those in the literature. The 2D algorithm is then modified and improved in such a way that it is valid for three-dimensional (3D) analysis in the case of random distributed fibres and inclusions. Linear interpolation of displacement field is employed to establish constraint equations of nodal displacements between two adjacent elements.

### 1.1 Constitutive equation, periodic condition, and meshing

1.1.1 Effective constitutive relations

For the transversely isotropic composite discussed this Section as shown in Figure 1, the effective constitutive relation of linear piezoelectricity, which is extensively used in the characterization of piezocomposites in this study, is defined as

$$
\begin{bmatrix} \bar{\sigma}_{11} \\ \bar{\sigma}_{22} \\ \bar{\sigma}_{33} \\ \bar{\sigma}_{23} \\ \bar{\sigma}_{31} \\ \bar{\sigma}_{12} \\ \bar{D}_1 \\ \bar{D}_2 \\ \bar{D}_3 \end{bmatrix} = \begin{bmatrix} c_{11}^{eff} & c_{12}^{eff} & c_{13}^{eff} & 0 & 0 & 0 & 0 & 0 & -e_{31}^{eff} \\ c_{12}^{eff} & c_{11}^{eff} & c_{13}^{eff} & 0 & 0 & 0 & 0 & 0 & -e_{31}^{eff} \\ c_{13}^{eff} & c_{13}^{eff} & c_{33}^{eff} & 0 & 0 & 0 & 0 & 0 & -e_{33}^{eff} \\ 0 & 0 & 0 & c_{44}^{eff} & 0 & 0 & 0 & -e_{15}^{eff} & 0 \\ 0 & 0 & 0 & 0 & c_{44}^{eff} & 0 & -e_{15}^{eff} & 0 & 0 \\ 0 & 0 & 0 & 0 & 0 & c_{66}^{eff} & 0 & 0 & 0 \\ 0 & 0 & 0 & 0 & e_{15}^{eff} & 0 & \kappa_{11}^{eff} & 0 & 0 \\ 0 & 0 & 0 & e_{15}^{eff} & 0 & 0 & 0 & \kappa_{11}^{eff} & 0 \\ e_{31}^{eff} & e_{31}^{eff} & e_{33}^{eff} & 0 & 0 & 0 & 0 & 0 & \kappa_{33}^{eff} \end{bmatrix} \begin{bmatrix} \bar{\varepsilon}_{11} \\ \bar{\varepsilon}_{22} \\ \bar{\varepsilon}_{33} \\ \bar{\varepsilon}_{23} \\ \bar{\varepsilon}_{31} \\ \bar{\varepsilon}_{12} \\ \bar{E}_1 \\ \bar{E}_2 \\ \bar{E}_3 \end{bmatrix}
$$

(1)

where $\sigma_{ij}$ is the stress tensor; $D_m$ the electric displacement; $E_m$ the electric field; $c_{ij}$ the elasticity tensor; $\kappa_{ik}$ the second order dielectric tensor; $e_{ik}$ the piezoelectric constant, and a bar over a variable here stands for volume average.
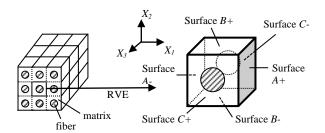


**Figure 1:** Schematic diagrams of periodic 1-3 composite laminate (a) and unit cell (b) (the fibre laminates are poled in $x_3$ direction)

The prediction of effective coefficients appeared in Eq (1) requires the adoption of periodic boundary conditions to generate appropriate loading.

### 1.1.2 Periodic Boundary Condition

As the homogeneous medium consists of periodic unit cells, periodic boundary conditions are required to apply on the boundaries of the RVE. The general periodic conditions expressed by Havner [12, 92] can be applied to ensure periodic displacement and subsequent stress field.

$$u_i(y) = u_i(y+Y)$$
$$\sigma_{ij}(y) = \sigma_{ij}(y+Y) \qquad (i,j=1,2,3) \qquad (2)$$

where $u_i$ denotes the displacement; $y$ represents any point in the periodic domain and $Y$ the periodicity. Applying this displacement condition to the boundary of the unit cell in Figure 1 yields.

$$u_i^{j+} = u_i^{j-} \qquad (i,j=1,2,3) \qquad (3)$$

which means the three-dimensional displacement vector for any pair of corresponding locations on areas A-/A+, B-/B+ and C-/C+ should be the same. A more explicit periodic boundary condition is then given as[12]

$$u_i = \bar{S}_{ij} x_j + v_i \qquad (4)$$

where the average strain $\bar{S}_{ij}$ is included as an arbitrarily imposed constant strain; $v_i$ denotes the periodic part of displacement component, which depends on the global loadings.

Based on the boundary condition (4), a unified periodic boundary condition can be given [12]:

$$u_i^{j+}(x,y,z) - u_i^{j-}(x,y,z) = c_i^j \ (i, j = 1, 2, 3) \qquad (5)$$
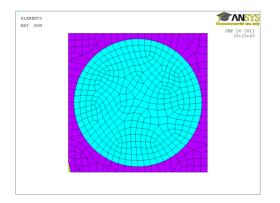
In the Eq. (5) above, for the constant terms on the right side of the equation, $c_1^1$, $c_2^2$ and $c_3^3$ represent the normal loads which are either traction or compression; while, $c_1^2 = c_2^1$, $c_1^3 = c_3^1$ and $c_2^3 = c_3^2$ represent the in-plane shear load.

## 1.2 2D FE Modelling

Figure 1 illustrates the configuration of the homogeneity of continuous fibre reinforced 1-3 composite [10]. In this case, the cylindrical fibres are in square arrangement and poled along the $x_3$ direction. This RVE configuration will be the focus in this section.

### 1.2. 1 Element Type and Material Property

SOLID226 in ANSYS element library is used, which is a 20-node hexagonal shaped element type with 3-D displacement degree-of-freedom (DoF) and additional voltage degree of freedom. This element type is easy for the implementation of periodic boundary conditions. And in the later development of 3D model, this element type will be suitable as the meshing method used for irregular model is only valid with tetrahedral element. The material properties inputs are taken from Berger et al. [93].
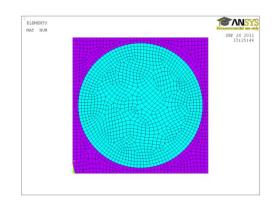




**Figure 2:** Different meshing density when volume fraction is 0.666. The RVE edge line is set into (a) 20 (b) 40 divisions

### 1.2.2 Element Mesh

For meshing, the area geometry is generated first and then sweep mesh is used to further generate the volume. In this way, the meshing result on C+/C- is the same. In addition, with the setting of the RVE edge line divisions, meshing results on A+/A- and B+/B- are also the same. Ultimately, this provides explicit convenience to imposing periodic boundary conditions. As illustrated, when dealing with the situation when volume fraction is specified, say 0.666, the outline of the fibre circle is much closer to the RVE edge; in this case, a lower density of element as shown Figure 2 (a) is not sufficient for accurate analysis since the elements between boundary of the RVE and the fibre have been lessened and shown distortion. When the edge division is 40 indicated in Figure 2 (b), the meshing quality is significantly improved.

As for periodic boundary condition, specific boundary conditions will be assigned to the exact opposite positions, namely A+/A-, B+/B- and C+/C-. For example, in x-direction

$$u_i(x^{A+}, y_j, z_j) - u_i(x^{A-}, y_k, z_k) = c \qquad (6)$$

where the subscripts j and k are the node number of any pair of nodes on opposite locations, A+ and A- area, respectively. The boundary conditions are shown in Figure 3.
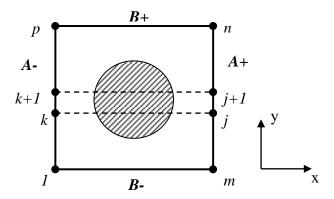
**Figure 3:** Application of periodic boundary conditions from a coordinate's view

Since the meshing scheme has ensured that there exists a pair of corresponding nodes at the opposite positions, the problem lies in developing a method to apply constraint equations on each pair of node for overcoming the problem of time-consuming over the node pair selection by graphical users' interface. An internal programme has thus been designed for accomplishing the task. The procedures of the implementation are described as follows:

**a**) Define the area A+, B+ and C+ as master areas, while A-, B- and C- as slave areas. Establish two arrays containing the node number (j, k) and coordinates ($y_{j,k}$, $z_{j,k}$) of each node (the x coordinate is not necessary, because the nodes are located on A+ and A- areas where the x coordinate is a constant).
**b**) Start from the first node in master array; get the node number j;
**c**)Use the coordinates ($y_j$, $z_j$) of the node j to find the node at the exact opposite location, $y_j = y_k$; $z_j = z_k$; and select the node k from the slave array.
**d**)Given the node number of the nodes on opposite location, constraint equations could be established.
The same procedures are adopted on B+/B- and C+/C- areas, whilst the coordinates obtained and stored will be X/Z and X/Y, respectively.

When integrating the constraint equations in three directions, special care has been taken to avoid over-constraint over the edges that connect areas A+/A-, B+/B- and C+/C-. Over-constraint may occur when the degree-of-freedom of one node is specified more than once. For example, when applying x-y in-plane shear load via constraint equations as shown in Figure 4, based on the periodic boundary conditions for A+/A-, the DoF relations between node 1 and 2 are $u_2 = u_1$ and $v_2 = v_1 + c$

while as to areas B+/B-, there will be relations between nodes 2 and 3 that $u_2 = u_3 + c$ and $v_2 = v_3$; the same problem will also occur in node 3. In this case, when applying constraint equations over B+/B-, the corner nodes of the RVE will be excluded to avoid over-constraint.
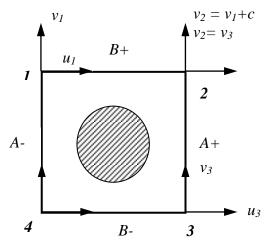


**Figure 4:** Over-constraint situations for 2-D mode

## II. RESULTS AND DISCUSSION

### 1. Numerical results of effective coefficients

Proper boundary conditions with strain load are specified pertaining to the calculation of different coefficients. For example, for the calculation of $c_{11}$ and $c_{12}$, the boundary conditions are applied in such a way that, except for the average normal strain in x direction $\varepsilon_{11}$, all the other mechanical and electric strain components are set to be zero. By this means, in Eq. (1), stiffness tensor $c_{11}$ and $c_{12}$ can be derived by
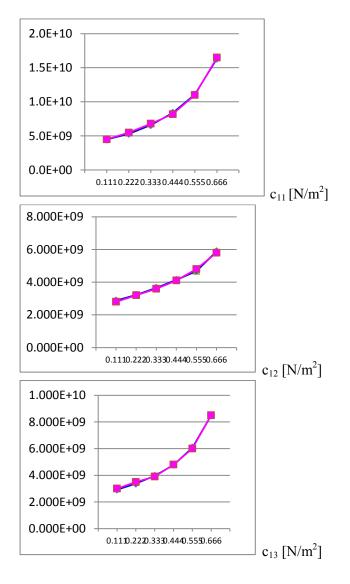
$$\bar{\sigma}_{11} = c_{11}^{eff} \bar{\varepsilon}_{11} \ ; \ \ \bar{\sigma}_{22} = c_{12}^{eff} \bar{\varepsilon}_{11} \tag{7}$$

Practically, this is achieved by setting the x-displacement on A-, y-displacement on B+/B- areas, and z-displacement on C+/C- areas to be zero; electric field on all areas to be zero. If we adopt periodic boundary conditions discussed before to A+/A-, where $u_x(A-) = 0$, the periodic boundary condition in Eq. (5) is simplified to

$$u_x(x^{A+}, y, z) = c_x^A \tag{8}$$

which indicates that all nodes on A+ area will present a displacement c in x+ direction. The calculation of other coefficients follows a same routine.

The numerical results obtained are shown in Figure 5 and compared with the FE results from Berger et al. [93]. The blue curve shows the data results from this work and the pink curve as the results in Berger et al. [93]. The curves shown in Figure 5 indicated a good match pertaining to elastic tensors, except for $c_{44}$ when the fibre volume fraction exceeds 0.444. Since the calculation of $c_{44}$ is highly dependent on the out-of-plane shear strain $\varepsilon_{23}$, and the implementation of such strain requires the original form of periodic boundary conditions rather than a normal displacement applied on one area when calculating $c_{11}$, $c_{12}$, $c_{13}$ and $c_{33}$, the accuracy of $c_{44}$ is significantly dependent on the meshing density than others.



$c_{11}$ [N/m$^2$]



$c_{12}$ [N/m$^2$]



$c_{13}$ [N/m$^2$]
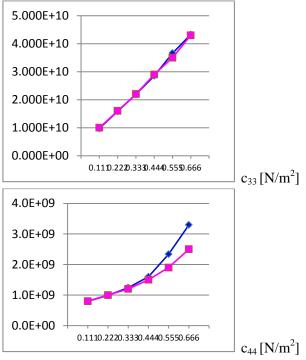


$c_{33}$ [N/m$^2$]



$c_{44}$ [N/m$^2$]

**Figure 5:** Numerical results of effective coefficients

## 2. Boundary elements for piezoelectric materials

### 2.1 Green functions for a hole embedded in an infinite piezoelectric solid

Consider a hole embedded in an infinite piezoelectric solid subjected to a line temperature discontinuity located at a point ($x_{10}$, $x_{20}$). Green functions for such a problem have been given in [45]. They are:

$$T = 2\,\mathrm{Re}[g'(z_t)] = 2\,\mathrm{Re}[f_0(\zeta_t) + f_1(\zeta_t)] \qquad (9)$$

$$\vartheta = -2\,\mathrm{Re}[ikg'(z_t)] = -2\,\mathrm{Re}[ikf_0(\zeta_t) + ikf_1(\zeta_t)] \,(10)$$

$$\mathbf{u} = 2\,\mathrm{Re}\{-\mathbf{A}[\mathbf{F}_1(\boldsymbol{\zeta}) + \mathbf{F}_2(\boldsymbol{\zeta})\mathbf{P}^{-1}\overline{\tau}]\mathbf{B}^{-1}\overline{\mathbf{d}} + \mathbf{c}g(\zeta_t)\} \quad (11)$$

$$\boldsymbol{\phi} = 2\,\mathrm{Re}\{-\mathbf{B}[\mathbf{F}_1(\boldsymbol{\zeta}) + \mathbf{F}_2(\boldsymbol{\zeta})\mathbf{P}^{-1}\overline{\tau}]\mathbf{B}^{-1}\overline{\mathbf{d}} + \mathbf{d}g(\zeta_t)\} \quad (12)$$

where T, $\vartheta$, $\mathbf{u}$ and $\boldsymbol{\phi}$ represent temperature, heat-flow function, EDEP and SED function vectors, respectively. $i = \sqrt{-1}$, "Re" represents the real part of a complex number, $\boldsymbol{\zeta} = \{\zeta_1 \ \zeta_2 \ \zeta_3 \ \zeta_4\}^T$, $\mathbf{P} = \mathrm{diag}\ [p_1 \ p_2 \ p_3 \ p_4]$, $\tau$ and $p_k$ are heat and electro-elastic eigen values of the materials whose imaginary parts are positive. $k = \sqrt{k_{11}k_{22} - k_{12}^2}$, where $k_{ij}$ is the thermal conductivity, $\mathbf{A}$, $\mathbf{B}$, $\mathbf{c}$ and $\mathbf{d}$ are the material eigenvector matrices and vectors which are defined in the literature (see [10], for example). $\zeta_k$ and $\zeta_t$ are related to the complex variables $z_k (= x_1 + p_k x_2)$ and $z_t (= x_1 + \tau x_2)$ by, respectively

$$z_k = a(a_{1k}\zeta_k + a_{2k}\zeta_k^{-1} + e_{n1}a_{3k}\zeta_k^n + e_{n1}a_{4k}\zeta_k^{-n}) \qquad (13)$$

$$z_t = a(a_{1\tau}\zeta_t + a_{2\tau}\zeta_t^{-1} + e_{n1}a_{3\tau}\zeta_t^n + e_{n1}a_{4\tau}\zeta_t^{-n}) \qquad (14)$$

in which

$$a_{1k} = (1-ip_ke)/2, \ a_{2k} = (1+ip_ke)/2, \\ a_{3k} = \gamma(1+ip_ke)/2, \ a_{4k} = \gamma(1-ip_ke)/2 \qquad (15)$$
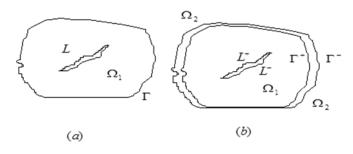
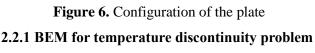$$a_{1\tau} = (1-i\tau e)/2, \ a_{2\tau} = (1+i\tau e)/2 \\ a_{3\tau} = \gamma(1+i\tau e)/2, \ a_{4\tau} = \gamma(1-i\tau e)/2 \qquad (8)$$

where $e_{ij} = 1$ if $i \neq j$; $e_{ij} = 0$ if $i = j$, $0 < e \leq 1$, n is an integer and has the same value for both subscript and argument of the functions. $\gamma$ and a are real parameters. By an appropriate selection of the parameters e, n and $\gamma$, we can obtain various kinds of cavities or holes, such as ellipse (n=1), circle (n=e=1), triangular (n=2), square (n=3) and pentagon (n=4). The functions $f_0$, $f_1$, $\mathbf{F}_1$, $\mathbf{F}_2$ and $g_t$ can be found in [8]. With the above solutions, the heat flow $h_i$ and SED $\Pi_i$ ( $= \{\sigma_{1i} \ \sigma_{2i} \ \sigma_{3i} \ D_i\}^T$ ) are calculated by the relations:

$$h_1 = -\vartheta_{,2}, \ h_2 = \vartheta_{,1}, \quad \mathbf{\Pi}_1 = -\phi_{,2}, \quad \mathbf{\Pi}_2 = \phi_{,1} \qquad (16)$$

where $h_i$, $\sigma_{ij}$ and $D_i$ are, respectively, heat flow, stress and electric displacement.

## 2.2 BEM for thermopiezoelectric problem

Consider again a 2D thermopiezoelectric solid inside of which there exist a hole and a number of cracks with arbitrary orientation and size. The numerical approach to such a problem usually involves the following steps. (i) Solve a heat transfer problem first to obtain the steady-state T field. (ii) Calculate the electroelastic field caused by the T field, then plus an isothermal solution to satisfy the corresponding mechanical boundary conditions. (iii) Finally, solve the modified problem for electroelastic fields. Unlike in the finite elements [94-105], we need to discretise the boundary only. In what follows, we begin by deriving the variational principle for temperature discontinuity and then extend it to the case of thermo-electroelasticity.



**Figure 6.** Configuration of the plate

### 2.2.1 BEM for temperature discontinuity problem

Let us consider a finite region $\Omega_1$ bounded by $\Gamma(= \Gamma_h + \Gamma_T)$ , as shown in Fig. 6(a). The heat transfer problem to be considered is stated as:

$$k_{ij}T_{,ij} = 0 \qquad \text{in } \Omega_1 \qquad (17)$$
$$h_n = h_i n_i = h_0 \qquad \text{on } \Gamma_h \qquad (18)$$
$$T = T_0 \qquad \text{on } \Gamma_T \qquad (19)$$
$$h_i n_i = 0 \qquad \text{on L} \qquad (20)$$

where $n_i$ is the normal to the boundary $\Gamma$, $h_0$ and $T_0$ are the prescribed values of heat flow and temperature, which act on the boundaries $\Gamma_h$ and $\Gamma_T$, respectively. For simplicity, we define $\hat{T} = T|_{L^+} - T|_{L^-}$ on L ($=L^+ + L^-$), where $\hat{T}$ is the temperature discontinuity, L is the union of all cracks, $L^+$ and $L^-$ are defined in Fig. 6(b). It should be pointed out that the boundary condition along the hole is automatically satisfied due to the use of the Green function given in Eqs. (9) and (10). Naturally, the hole boundary condition is not involved in the following analysis.

Further, if we let $\Omega_2$ be the complementary region of $\Omega_1$ (i.e., the union of $\Omega_1$ and $\Omega_2$ forms the infinite region $\Omega$) and $\hat{T} = T|_{\Gamma^+} - T|_{\Gamma^-} = T_0$ , the problem shown in Fig 4(a) can be extended to the infinite case (see Fig. 6b). Here $\Gamma = \Gamma^+ + \Gamma^-$ , where $\Gamma^+$ and $\Gamma^-$ stand for the boundaries of $\Omega_1$ and $\Omega_2$, respectively [see Fig. 6(b)]. In a way similar to that in [8], the total generalised potential energy for the thermal problem defined above is given by:

$$P(T,\hat{T}) = \frac{1}{2}\int_\Omega k_{ij}T_{,i}T_{,j}d\Omega + \int_\Gamma h_n\hat{T}dL \qquad (21)$$

By transforming the area integral in Eq. (21) to a boundary integral, we have

$$P(T,\hat{T}) = -\frac{1}{2}\int_L \vartheta(T)\hat{T}_{,s}ds + \int_\Gamma h_n\hat{T}ds \tag{22}$$

in which the relation

$$h_i = -k_{ij}T_{,j} \text{ and } \int_L h_n\hat{T}ds = \int_L [(\vartheta\hat{T})_{,s} - \vartheta\hat{T}_{,s}]ds \tag{23}$$

and the temperature discontinuity is assumed to be continuous over L and zero at the ends of L. Moreover, temperature T in Eq. (22) can be expressed in terms of $\hat{T}$ through use of Eq. (9). Therefore, the potential energy can be further written as

$$P(\hat{T}) = -\frac{1}{2}\int_L \vartheta(\hat{T})\hat{T}_{,s}ds + \int_\Gamma h_n\hat{T}ds \tag{24}$$

The analytical results for the minimum of potential (24) is not, in general, possible, and therefore a numerical procedure must be used to solve the problem. As in conventional BEM, the boundaries $\Gamma$ and L are divided into a series of linear boundary elements for which the temperature discontinuity may be approximated by a linear function. To illustrate this, take a particular element m, which is a line connected by nodes m and m+1, as an example (see Fig. 7)

$$\hat{T}(s) = \hat{T}_m F_m(s) + \hat{T}_{m+1}F_{m+1}(s) \tag{25}$$

where $\hat{T}_m$ is the temperature discontinuity at node m, and functions $F_m(s)$, $F_{m+1}(s)$ are shown in Figure 7.
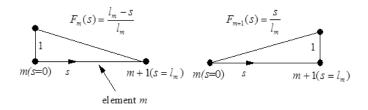


**Figure 7.** The definitions of $F_m(s)$ and $F_{m+1}(s)$

On the use of Eqs. (9), (10) and (25), the temperature and heat-flux function at point $z_t$ are

$$T(z_t) = \sum_{m=1}^M \text{Im}[a_m(z_t)]\hat{T}_m \tag{26}$$

$$\vartheta(z_t) = -k\sum_{m=1}^M \text{Re}[a_m(z_t)]\hat{T}_m \tag{27}$$

where M is the total number of nodes, "Im" represents the imaginary part of a complex number, and

$$a_m(\zeta_t) = \frac{1}{2\pi}\int_{l_{m-1}}\{\ln(\zeta_t - \zeta_{t0}^{m-1}) + \ln(\zeta_t^{-1} - \bar{\zeta}_{t0}^{m-1})\}\frac{l_{m-1}-s}{l_{m-1}}ds$$
$$+ \frac{1}{2\pi}\int_{l_m}\{\ln(\zeta_t - \zeta_{t0}^m) + \ln(\zeta_t^{-1} - \bar{\zeta}_{t0}^m)\}\frac{s}{l_m}ds$$

(28)

in which $\zeta_{t0}$ can be expressed in terms of s by the relations

$$z_t = f(\zeta_t) = a(a_{1\tau}\zeta_t + a_{2\tau}\zeta_t^{-1} + e_{n1}a_{3\tau}\zeta_t^n + e_{n1}a_{4\tau}\zeta_t^{-n}), \tag{29}$$

$$\zeta_{t0}^{m-1} = f^{-1}(z_{t0}^{m-1}), \qquad \zeta_{t0}^m = f^{-1}(z_{t0}^m), \tag{30}$$

$$z_{t0}^{m-1} = d_m + s(\cos\alpha_{m-1} + \tau\sin\alpha_{m-1}),$$
$$z_{t0}^m = d_m + s(\cos\alpha_m + \tau\sin\alpha_m) \tag{31}$$

and $d_m = x_{1m} + \tau x_{2m}$, $(x_{1m}, x_{2m})$ is the coordinates at node m, $\alpha_m$ is the angle between the element m and $x_1$-axis, $\alpha_{m-1}$ is defined similarly. It should be pointed out that the solution of $\zeta_{t0}$ in Eq. (30) is multi-valued, as there exist n-roots located outside the unit circle [46]. The root whose magnitude has a minimum value is chosen in our analysis [46].

Using Eq. (26), the temperature at node j can be written as

$$T_j(\zeta_{tj}) = \sum_{m=1}^M \text{Im}[a_m(\zeta_{tj})]\hat{T}_m \tag{32}$$

Substituting Eq. (25) into Eq. (24) yields

$$P(\hat{T}) \approx \sum_{j=1}^M[\sum_{m=1}^M (-\frac{1}{2}K_{mj}\hat{T}_m\hat{T}_j) + G_j\hat{T}_j] \tag{33}$$

where $K_{mj}$ is known as the stiffness matrix and $G_j$ the equivalent nodal heat flux vector, which are given by:

$$K_{mj} = -\frac{k}{l_{j-1}}\int_{l_{j-1}} \text{Re}[a_m(\zeta_{t0}^{j-1})]ds + \frac{k}{l_j}\int_{l_j} \text{Re}[a_m(\zeta_{t0}^j)]ds \tag{34}$$

$$G_j = \int_{l_{j-1}+l_j} h_{*0}F_j(s)ds \tag{35}$$

The minimization of $P(\hat{T})$ yields

$$\sum_{j=1}^M K_{mj}\hat{T}_j = G_m \tag{36}$$

The final form of the linear equations to be solved is obtained by selecting the appropriate ones, from among Eqs. (32) and (36). Eq. (32) will be chosen for those nodes at which the temperature is prescribed, and Eq. (36) for the remaining nodes. After the nodal temperature discontinuities have been calculated, the EDEP and SED at any point in the region can be evaluated by using Eqs. (11), (12) and (16). They are

$$\mathbf{u} = \sum_{j=1}^M \mathbf{w}_j\hat{T}_j, \quad \Pi_1 = \sum_{j=1}^M \mathbf{x}_j\hat{T}_j, \quad \Pi_2 = \sum_{j=1}^M \mathbf{y}_j\hat{T}_j \tag{37}$$

where

$$\mathbf{w}_j = -\frac{1}{2\pi}\mathrm{Im}\{\int_{l_{j-1}}[\mathbf{A}(\mathbf{F}_1(\boldsymbol{\zeta})+\mathbf{F}_2(\boldsymbol{\zeta})\mathbf{P}^{-1}\bar{\tau})\mathbf{B}^{-1}\bar{\mathbf{d}}-\mathbf{c}g(\zeta_t)]\frac{l_{j-1}-s}{l_{j-1}}ds\}$$

$$-\frac{1}{2\pi}\mathrm{Im}\{\int_{l_j}[\mathbf{A}(\mathbf{F}_1(\boldsymbol{\zeta})+\mathbf{F}_2(\boldsymbol{\zeta})\mathbf{P}^{-1}\bar{\tau})\mathbf{B}^{-1}\bar{\mathbf{d}}-\mathbf{c}g(\zeta_t)]\frac{s}{l_j}ds\}$$

$$(38)$$

$$\mathbf{x}_j = \frac{1}{2\pi}\mathrm{Im}\{\int_{l_{j-1}}[\mathbf{B}(\mathbf{F}_1'(\boldsymbol{\zeta})\mathbf{P}+\mathbf{F}_2'(\boldsymbol{\zeta})\bar{\tau})\mathbf{B}^{-1}\bar{\mathbf{d}}-\mathbf{c}\tau g'(\zeta_t)]\frac{l_{j-1}-s}{l_{j-1}}ds\}$$

$$+\frac{1}{2\pi}\mathrm{Im}\{\int_{l_j}[\mathbf{B}(\mathbf{F}_1'(\boldsymbol{\zeta})\mathbf{P}+\mathbf{F}_2'(\boldsymbol{\zeta})\bar{\tau})\mathbf{B}^{-1}\bar{\mathbf{d}}-\mathbf{c}\tau g'(\zeta_t)]\frac{s}{l_j}ds\}$$

$$(39)$$

$$\mathbf{y}_j = -\frac{1}{2\pi}\mathrm{Im}\{\int_{l_{j-1}}[\mathbf{B}(\mathbf{F}_1'(\boldsymbol{\zeta})+\mathbf{F}_2'(\boldsymbol{\zeta})\mathbf{P}^{-1}\bar{\tau})\mathbf{B}^{-1}\bar{\mathbf{d}}-\mathbf{c}g'(\zeta_t)]\frac{l_{j-1}-s}{l_{j-1}}ds\}$$

$$-\frac{1}{2\pi}\mathrm{Im}\{\int_{l_j}[\mathbf{B}(\mathbf{F}_1'(\boldsymbol{\zeta})+\mathbf{F}_2'(\boldsymbol{\zeta})\mathbf{P}^{-1}\bar{\tau})\mathbf{B}^{-1}\bar{\mathbf{d}}-\mathbf{c}g'(\zeta_t)]\frac{s}{l_j}ds\}$$

$$(40)$$

Thus, the surface traction-charge and EDEP induced by the temperature discontinuity are of the form

$$\mathbf{t}_n^0(s) = \Pi_i n_i = \sum_{j=1}^{M}(\mathbf{x}_j n_1 + \mathbf{y}_j n_2)\hat{T}_j, \quad \mathbf{u}_*^0(s) = \sum_{j=1}^{M}\mathbf{w}_j(s)\hat{T}_j \quad (41)$$

In general, $\mathbf{t}_n^0(s) \neq 0$ over $\Gamma_t$ (the boundary on which SED is prescribed) and $\mathbf{u}_*^0(s) \neq 0$ over $\Gamma_u$ (the boundary on which EDEP is prescribed). To satisfy the SED (or EDEP) on the corresponding boundaries, we must superpose a solution of the corresponding isothermal problem with a SED (or a EDEP) equal and opposite to those of Eq. (41). The details will be given in the following sub-section.

## 22.2 BEM for EDEP Discontinuity Problem

Consider again the domain $\Omega_1$, the governing equation and its boundary conditions are described as follows

$$\Pi_{ij,j} = 0 \quad \text{in } \Omega_1 \quad (42)$$

$$t_{ni} = \Pi_{ij}n_j = t_i^0 - (\mathbf{t}_n^0)_i \quad \text{on } \Gamma_t \quad (43)$$

$$u_i = u_i^0 - (\mathbf{u}_*^0)_i \quad \text{on } \Gamma_u \quad (44)$$

$$t_{ni}|_{L^+} = -t_{ni}|_{L^-} = -(\mathbf{t}_n^0)_i,$$
$$\hat{u}_i = u_i|_{L^+} - u_i|_{L^-} - (\mathbf{u}_*^0)_i|_{L^+} + (\mathbf{u}_*^0)_i|_{L^-} \quad \text{on } L \quad (45)$$

where $\Gamma_t$ and $\Gamma_u$ are the boundaries on which the prescribed values of SED $t_i^0$ and EDEP $u_i^0$ are imposed, and $\Pi_{ij} = (\mathbf{\Pi}_j)_i$. Similarly, the total potential energy for the electroelastic problem can be given as

$$\Pi(\hat{\mathbf{u}}) = \frac{1}{2}\int_L[\boldsymbol{\phi}(\hat{\mathbf{u}})\cdot\hat{\mathbf{u}}_{,s} + 2\mathbf{t}_n^0\cdot\hat{\mathbf{u}}]ds - \int_\Gamma(\mathbf{t}^0 - \mathbf{t}_n^0)\cdot\hat{\mathbf{u}}ds \quad (46)$$

where the elastic solutions of the functions $\boldsymbol{\phi}(\hat{\mathbf{u}})$ and $\mathbf{u}(\hat{\mathbf{u}})$ have been given in [46]. These solutions are:

$$\mathbf{u}(\hat{\mathbf{u}}) = \frac{1}{\pi}\mathrm{Im}[\mathbf{A}\langle\ln(\zeta_\alpha - \zeta_{\alpha 0})\rangle\mathbf{B}^T\hat{\mathbf{u}}$$
$$+\frac{1}{\pi}\sum_{\beta=1}^{4}\mathrm{Im}[\mathbf{A}\langle\ln(\zeta_\alpha^{-1} - \bar{\zeta}_{\beta 0})\rangle\mathbf{B}^{-1}\bar{\mathbf{B}}\mathbf{I}_\beta\bar{\mathbf{B}}^T\hat{\mathbf{u}}$$

$$(47)$$

$$\boldsymbol{\phi}(\hat{\mathbf{u}}) = \frac{1}{\pi}\mathrm{Im}[\mathbf{B}\langle\ln(\zeta_\alpha - \zeta_{\alpha 0})\rangle\mathbf{B}^T\hat{\mathbf{u}}$$
$$+\frac{1}{\pi}\sum_{\beta=1}^{4}\mathrm{Im}[\mathbf{B}\langle\ln(\zeta_\alpha^{-1} - \bar{\zeta}_{\beta 0})\rangle\mathbf{B}^{-1}\bar{\mathbf{B}}\mathbf{I}_\beta\bar{\mathbf{B}}^T\hat{\mathbf{u}}$$

$$(48)$$

where

$$\mathbf{I}_1 = \mathrm{diag}[1,0,0,0], \quad \mathbf{I}_2 = \mathrm{diag}[0,1,0,0],$$
$$\mathbf{I}_3 = \mathrm{diag}[0,0,1,0], \quad \mathbf{I}_4 = \mathrm{diag}[0,0,0,1] \quad (49)$$

As before the boundaries L and $\Gamma$ are divided into a series of boundary elements, for which the EDEP discontinuity may be approximated through linear interpolation as

$$\hat{\mathbf{u}}(s) = \hat{\mathbf{u}}_m F_m(s) + \hat{\mathbf{u}}_{m+1}F_{m+1}(s) \quad (50)$$

With approximation (50), the EDEP and SED functions given in Eqs. (47) and (48) can now be expressed by

$$\mathbf{u}(\boldsymbol{\zeta}) = \sum_{m=1}^{M}\mathrm{Im}[\mathbf{AD}_m(\boldsymbol{\zeta})]\hat{\mathbf{u}}_m, \quad \boldsymbol{\phi}(\boldsymbol{\zeta}) = \sum_{m=1}^{M}\mathrm{Im}[\mathbf{BD}_m(\boldsymbol{\zeta})]\hat{\mathbf{u}}_m \quad (51)$$

where

$$\mathbf{D}_m(\boldsymbol{\zeta}) = \frac{1}{\pi}\int_{l_{m-1}}\{\langle\ln(\zeta_\alpha - \zeta_{\alpha 0}^{m-1})\rangle\mathbf{B}^T + \sum_{\beta=1}^{4}\langle\ln(\zeta_\alpha^{-1} - \bar{\zeta}_{\beta 0}^{m-1})\rangle\mathbf{B}^{-1}\bar{\mathbf{B}}\mathbf{I}_\beta\bar{\mathbf{B}}^T\}\frac{l_{m-1}-s}{l_{m-1}}ds$$

$$+\frac{1}{\pi}\int_{l_m}\{\langle\ln(\zeta_\alpha - \zeta_{\alpha 0}^{m})\rangle\mathbf{B}^T + \sum_{\beta=1}^{4}\langle\ln(\zeta_\alpha^{-1} - \bar{\zeta}_{\beta 0}^{m})\rangle\mathbf{B}^{-1}\bar{\mathbf{B}}\mathbf{I}_\beta\bar{\mathbf{B}}^T\}\frac{s}{l_m}ds$$

$$(52)$$

in which $\zeta_t$ and $\zeta_{t0}$ can be expressed in terms of s by the relations

$$z_\alpha = f(\zeta_\alpha) = a(a_{1\alpha}\zeta_\alpha + a_{2\alpha}\zeta_\alpha^{-1} + e_{n1}a_{3\alpha}\zeta_\alpha^n + e_{n1}a_{4\alpha}\zeta_\alpha^{-n}) \quad (53)$$

$$\zeta_{\alpha 0}^{m-1} = f^{-1}(z_{\alpha 0}^{m-1}), \quad \zeta_{\alpha 0}^m = f^{-1}(z_{\alpha 0}^m), \quad (54)$$

$$z_{\alpha 0}^{m-1} = d_{\alpha m} + s(\cos\alpha_{m-1} + p_\alpha\sin\alpha_{m-1}),$$
$$z_{\alpha 0}^m = d_{\alpha m} + s(\cos\alpha_m + p_\alpha\sin\alpha_m) \quad (55)$$

and $d_{\alpha m} = x_{1m} + p_\alpha x_{2m}$.

In particular the displacement at node j is given by

$$\mathbf{u}(\zeta_0^j) = \sum_{m=1}^{M}\mathrm{Im}[\mathbf{AD}_m(\zeta_0^j)]\hat{\mathbf{u}}_m, \quad (56)$$

Substituting Eq. (44) into Eq. (39), we have

$$\Pi(\hat{\mathbf{u}}) = \sum_{i=1}^{M}[\hat{\mathbf{u}}_i^T\cdot(\sum_{j=1}^{M}\mathbf{k}_{ij}\hat{\mathbf{u}}_j)/2 - \mathbf{g}_i] \quad (57)$$

where

$$\mathbf{k}_{ij} = \frac{1}{l_{j-1}} \int_{l_{j-1}} \text{Im}[\mathbf{D}_i^T(\boldsymbol{\zeta}_0^{j-1})\mathbf{B}^T] ds - \frac{1}{l_j} \int_{l_j} \text{Im}[\mathbf{D}_i^T(\boldsymbol{\zeta}_0^{j})\mathbf{B}^T] ds \quad (58)$$

$$\mathbf{g}_j = \int_{l_{j-1}+l_j} \mathbf{G}_j F_j(s) ds \quad (59)$$

and $\mathbf{G}_j = -\mathbf{t}_n^0$ when node j is located at the boundary L, $\mathbf{G}_j = \mathbf{t}^0 - \mathbf{t}_n^0$ for other nodes. The minimization of Eq. (57) leads to a set of linear equations

$$\sum_{j=1}^{M} \mathbf{K}_{ij} \hat{\mathbf{u}}_j = \mathbf{g}_i \quad (60)$$

Similarly, the final form of the linear equations to be solved is obtained by selecting the appropriate ones, from among Eqs. (56) and (60). Eq. (56) will be chosen for those nodes at which the EDEP is prescribed, and Eq. (60) for the other nodes. Once the EDEP discontinuity $\hat{\mathbf{u}}$ has been found, the SED at any point can be expressed by:

$$\Pi_1 = -\sum_{m=1}^{M} \text{Im}[\mathbf{BPD}'_m(\mathbf{z})\hat{\mathbf{u}}_m], \ \Pi_2 = \sum_{m=1}^{M} \text{Im}[\mathbf{BD}'_m(\mathbf{z})\hat{\mathbf{u}}_m] \quad (61)$$

Therefore the SED, $\Pi_n$, in a coordinate system local to the crack line, is given by

$$\Pi_n = \Phi(\alpha)\{-\Pi_1 \sin\alpha + \Pi_2 \cos\alpha\}^T \quad (62)$$

where $\Phi(\alpha)$ is defined by[4]

$$\Phi(\alpha) = \begin{bmatrix} \cos\alpha & \sin\alpha & 0 & 0 \\ -\sin\alpha & \cos\alpha & 0 & 0 \\ 0 & 0 & 1 & 0 \\ 0 & 0 & 0 & 1 \end{bmatrix} \quad (63)$$

Using Eq. (62) we can evaluate the SED intensity factors by the following definition

$$\mathbf{K}(c) = \{K_{II} \ K_I \ K_{III} \ K_D\}^T = \lim_{r \to 0} \sqrt{2\pi r} \Pi_n(r) \quad (64)$$

We can evaluate the SED intensity factors in several ways: by extrapolation, traction and J-integral formulae [15]. In our analysis, the first method is used to calculate the SED intensity factors in BEM. Here, $\Pi_n$ at any two points (say A and B) ahead of a crack-tip is first derived and then substituting them into Eq. (64), we obtain

$$\mathbf{K}^A = \sigma_n^A \sqrt{2\pi r_A}, \quad \mathbf{K}^B = \sigma_n^B \sqrt{2\pi r_B} \quad (65)$$

where $r_A$ (or $r_B$) are the distance from crack-tip to point A (or B). Finally, the SED intensity factors $\mathbf{K}$ can be obtained by the linear extrapolation of $\mathbf{K}^A$ and $\mathbf{K}^B$ to the crack tip, that is

$$\mathbf{K} = \mathbf{K}^A - \frac{\mathbf{K}^B - \mathbf{K}^A}{r_B - r_A} r_A \quad (66)$$

## III. CONCLUSIONS AND FUTURE DEVELOPMENTS

On the basis of the preceding discussion, following conclusions can be drawn. This review presents an overall view on evaluating overall properties of piezoelectric composites. It includes micromechanics calculation, boundary elements and finite element modeling.

It is recognized that study on piezoelectric materials becomes a hot topic and has become increasingly popular due their widely applications in engineering fields. However, there are still many possible extensions and areas in need of further development in the future. Among those developments one could list the following:

1. Development of efficient Trefftz finite element-boundary element method schemes for complex piezoelectric structures and the related general purpose computer codes with preprocessing and post processing capabilities.
2. Applications of piezoelectric composites to MEMS and smart devices and development of the associated design and fabrication approaches.
3. Extension of the Trefftz-finite element method to electrodynamics of piezoelectric structures, dynamics of thin and thick plate bending and fracture mechanics for structures containing piezoelectric sensor and actuators.
4. Development of multistate framework across from continuum to micro- and nano-scales for modeling piezoelectric materials and structures.

## IV. REFERENCES

[1] J. Curie, P. Curie, Development par compression de l'eletricite polaire dans les cristaux hemiedres a faces inclines, Comptes Rendus Acad. Sci. Paris, 91 (1880) 294.

[2] W. Voigt, General theory of the piezo-and pyroelectric properties of crystals, Abh. Gott, 36(1) (1890).

[3] W. Cady, Piezoelectricity, vols. 1 and 2, Dover Publishers, New York, 1964.

[4] H.F. Tiersten, Linear piezoelectric plate vibrations, Springer, New York, 1969.

[5] V.Z. Parton, B.A. Kudryavtsev, Electromagnetoelasticity: piezoelectrics and electrically conductive solids, Gordon and Breach Science Publishers, New York, 1988.

[6] T. Ikeda, Fundamentals of piezoelectricity, Oxford university press, New York, 1996.

[7] N.N. Rogacheva, The theory of piezoelectric shells and plates, CRC Press, Boca Raton, 1994.

[8] Q.H. Qin, Fracture mechanics of piezoelectric materials, WIT Press, Southampton, 2001.

[9] Q.H. Qin, Green's function and boundary elements of multifield materials, Elsevier, Oxford, 2007.

[10] Q.H. Qin, Advanced mechanics of piezoelectricity, Higher Education Press and Springer, Beijing, 2013.

[11] Q.H. Qin, Mechanics of Cellular Bone Remodeling: Coupled Thermal, Electrical, and Mechanical Field Effects, CRC Press, Taylor & Francis, Boca Raton, 2013.

[12] Q.H. Qin, Q.S. Yang, Macro-micro theory on multifield coupling behaivor of hetereogenous materials, Higher Education Press and Springer, Beijing, 2008.

[13] S. Diao, Q.H. Qin, J. Dong, On branched interface cracks between two piezoelectric materials, Mechanics research communications, 23(6) (1996) 615-620.

[14] Q.H. Qin, Y.W. Mai, Crack branch in piezoelectric bimaterial system, International Journal of Engineering Science, 38(6) (2000) 673-693.

[15] Q.H. Qin, X. Zhang, Crack deflection at an interface between dissimilar piezoelectric materials, International Journal of Fracture, 102(4) (2000) 355-370.

[16] D. Fu, Z. Hou, Q.H. Qin, L. Xu, Y. Zeng, Influence of Shear Stress on Behaviors of Piezoelectric Voltages in Bone, Journal of Applied Biomechanics, 28(4) (2012) 387-393.

[17] D.H. Fu, Z.D. Hou, Q.H. Qin, Analysis of the waveforms of piezoelectric voltage of bone, Journal of Tianjin University, 39 (2006) 349-353.

[18] D.H. Fu, Z.D. Hou, Q.H. Qin, Influence of a notch on the piezoelectric voltages in bone, Engineering Mechanics, 28(1) (2011) 233-237.

[19] D.H. Fu, Z.D. Hou, Q.H. Qin, C. Lu, On the Influence of Relative Humidity on Piezoelectric Signals in Bone, Journal of Experimental Mechanics, 24(5) (2009) 473-478.

[20] Z. Hou, D. Fu, Q.H. Qin, An exponential law for stretching–relaxation properties of bone piezovoltages, International Journal of Solids and Structures, 48(3) (2011) 603-610.

[21] L. Xu, Z. Hou, D. Fu, Q.-H. Qin, Y. Wang, Stretched exponential relaxation of piezovoltages in wet bovine bone, Journal of the Mechanical Behavior of Biomedical Materials, 41 (2015) 115-123.

[22] X. He, C. Qu, Q.H. Qin, A theoretical model for surface bone remodeling under electromagnetic loads, Archive of Applied Mechanics, 78(3) (2008) 163-175.

[23] Q.H. Qin, Thermoelectroelastic solutions for internal bone remodelling under constant loads, Mechanics of electromagnetic solids, 3 (2003) 73-88.

[24] Q.H. Qin, Multi-field bone remodeling under axial and transverse loads, in: D.R. Boomington (Ed.) New research on biomaterials, Nova Science Publishers, New York, 2007, pp. 49-91.

[25] Q.H. Qin, C. Qu, J. Ye, Thermoelectroelastic solutions for surface bone remodeling under axial and transverse loads, Biomaterials, 26(33) (2005) 6798-6810.

[26] Q.H. Qin, J.Q. Ye, Thermoelectroelastic solutions for internal bone remodeling under axial and transverse loads, International Journal of Solids and Structures, 41(9) (2004) 2447-2460.

[27] C. Qu, X. He, Q.H. Qin, Bone functional remodeling under multi-field loadings, Proceedings of the 5th Australasian Congress on Applied Mechanics, (2007) 627-632.

[28] C. Qu, Q.H. Qin, Bone remodeling under multi-field coupled loading, Zhineng Xitong Xuebao(CAAI Transactions on Intelligent Systems), 2(3) (2007) 52-58.

[29] C. Qu, Q.H. Qin, Y. Kang, A hypothetical mechanism of bone remodeling and modeling under electromagnetic loads, Biomaterials, 27(21) (2006) 4050-4057.

[30] X. He, J.S. Wang, Q.H. Qin, Saint-Venant decay analysis of FGPM laminates and dissimilar piezoelectric laminates, Mechanics of Materials, 39(12) (2007) 1053-1065.

[31] K.Q. Hu, Y.L. Kang, Q.H. Qin, A moving crack in a rectangular magnetoelectroelastic body, Engineering Fracture Mechanics, 74(5) (2007) 751-770.

[32] K.Q. Hu, Q.H. Qin, Y.L. Kang, Anti-plane shear crack in a magnetoelectroelastic layer sandwiched between dissimilar half spaces, Engineering Fracture Mechanics, 74(7) (2007) 1139-1147.

[33] Q.H. Qin, Solving anti-plane problems of piezoelectric materials by the Trefftz finite element

approach, Computational Mechanics, 31(6) (2003) 461-468.

[34] H.Y. Liu, Q.H. Qin, Y.W. Mai, Theoretical model of piezoelectric fibre pull-out, International Journal of Solids and Structures, 40(20) (2003) 5511-5519.

[35] Q.H. Qin, J.S. Wang, Y.L. Kang, A theoretical model for electroelastic analysis in piezoelectric fibre push-out test, Archive of Applied Mechanics, 75(8-9) (2006) 527-540.

[36] J.S. Wang, Q.H. Qin, Debonding criterion for the piezoelectric fibre push-out test, Philosophical Magazine Letters, 86(2) (2006) 123-136.

[37] J.S. Wang, Q.H. Qin, Y.L. Kang, Stress and electric field transfer of piezoelectric fibre push-out under electrical and mechanical loading, in: Proc. of 9th International Conference on Inspection, Appraisal, Repairs & Maintenance of Structures, Fuzhou, China, 20-21 October, CI-Premier PTY LTD, ISBN: 981-05-3548-1, 2005, pp. 435-442.

[38] Z. Liu, Z. Hou, Q.H. Qin, Y. Yu, L. Tang, On electromechanical behaviour of frog sartorius muscles, in: Engineering in Medicine and Biology Society, 2005. IEEE-EMBS 2005. 27th Annual International Conference of the, IEEE, 2006, pp. 1252-1255.

[39] Q.H. Qin, Using GSC theory for effective thermal expansion and pyroelectric coefficients of cracked piezoelectric solids, International Journal of Fracture, 82(3) (1996) R41-R46.

[40] Q.H. Qin, Y.W. Mai, S.W. Yu, Effective moduli for thermopiezoelectric materials with microcracks, International Journal of Fracture, 91(4) (1998) 359-371.

[41] Q.H. Qin, S.W. Yu, Effective moduli of piezoelectric material with microcavities, International Journal of Solids and Structures, 35(36) (1998) 5085-5095.

[42] Q.H. Qin, S.W. Yu, Using Mori-Tanaka method for effective moduli of cracked thermopiezoelectric materials, in: ICF 9-Sydney, Australia-1997, 1997.

[43] Q.H. Qin, Thermoelectroelastic Green's function for a piezoelectric plate containing an elliptic hole, Mechanics of Materials, 30(1) (1998) 21-29.

[44] Q.H. Qin, Thermoelectroelastic Green's function for thermal load inside or on the boundary of an elliptic inclusion, Mechanics of Materials, 31(10) (1999) 611-626.

[45] Q.H. Qin, Green's function for thermopiezoelectric plates with holes of various shapes, Archive of Applied Mechanics, 69(6) (1999) 406-418.

[46] Q.H. Qin, Green function and its application for a piezoelectric plate with various openings, Archive of Applied Mechanics, 69(2) (1999) 133-144.

[47] Q.H. Qin, Green's functions of magnetoelectroelastic solids with a half-plane boundary or bimaterial interface, Philosophical Magazine Letters, 84(12) (2004) 771-779.

[48] Q.H. Qin, 2D Green's functions of defective magnetoelectroelastic solids under thermal loading, Engineering Analysis with Boundary Elements, 29(6) (2005) 577-585.

[49] Q.H. Qin, Green's functions of magnetoelectroelastic solids and applications to fracture analysis, in: Proc. of 9th International Conference on Inspection, Appraisal, Repairs & Maintenance of Structures, Fuzhou, China, 20-21 October,2005, CI-Premier PTY LTD, ISBN: 981-05-3548-1, 2005, pp. 93-106.

[50] Q.H. Qin, Y.W. Mai, Thermoelectroelastic Green's function and its application for bimaterial of piezoelectric materials, Archive of Applied Mechanics, 68(6) (1998) 433-444.

[51] Q.H. Qin, General solutions for thermopiezoelectrics with various holes under thermal loading, International Journal of Solids and Structures, 37(39) (2000) 5561-5578.

[52] Q.H. Qin, Y.W. Mai, A new thermoelectroelastic solution for piezoelectric materials with various openings, Acta Mechanica, 138(1) (1999) 97-111.

[53] Q.H. Qin, Y.W. Mai, S.W. Yu, Some problems in plane thermopiezoelectric materials with holes, International Journal of Solids and Structures, 36(3) (1999) 427-439.

[54] Q.H. Qin, A new solution for thermopiezoelectric solid with an insulated elliptic hole, Acta Mechanica Sinica, 14(2) (1998) 157-170.

[55] Q.H. Qin, General solutions for thermopiezoelectric materials with various openings, Encyclopedia of Thermal Stresses, (2014) 1932-1942.

[56] Q.H. Qin, Thermoelectroelastic analysis of cracks in piezoelectric half-plane by BEM, Computational Mechanics, 23(4) (1999) 353-360.

[57] Q.H. Qin, Material properties of piezoelectric composites by BEM and homogenization method, Composite structures, 66(1) (2004) 295-299.

[58] Q.H. Qin, Micromechanics-BE solution for properties of piezoelectric materials with defects, Engineering Analysis with Boundary Elements, 28(7) (2004) 809-814.

[59] Q.H. Qin, Micromechanics-BEM Analysis for Piezoelectric Composites, Tsinghua Science & Technology, 10(1) (2005) 30-34.

[60] Q.H. Qin, Boundary Element Method, in: J.S. Yang (Ed.) Special Topics in the Theory of Piezoelectricity, Springer, Cambridge Massachusetts, 2009, pp. 137-168.

[61] Q.H. Qin, Analysis of Piezoelectric Solids through Boundary Element Method, J Appl Mech Eng, 2(1) (2012) e113.

[62] Q.H. Qin, Y.W. Mai, BEM for crack-hole problems in thermopiezoelectric materials, Engineering Fracture Mechanics, 69(5) (2002) 577-588.

[63] Q.H. Qin, Mode III fracture analysis of piezoelectric materials by Trefftz BEM, Structural Engineering and Mechanics, 20(2) (2005) 225-240.

[64] Q.H. Qin, Thermopiezoelectric interaction of macro- and micro-cracks in piezoelectric medium, Theoretical and Applied Fracture Mechanics, 32(2) (1999) 129-135.

[65] Q.H. Qin, Variational formulations for TFEM of piezoelectricity, International Journal of Solids and Structures, 40(23) (2003) 6335-6346.

[66] Q.H. Qin, Fracture Analysis of Piezoelectric Materials by Boundary and Trefftz Finite Element Methods, WCCM VI in conjunction with APCOM'04, Sept. 5-10, 2004, Beijing, China, (2004).

[67] Q.H. Qin, Trefftz Plane Element of Piezoelectric Plate with p-Extension Capabilities, IUTAM Symposium on Mechanics and Reliability of Actuating Materials, (2006) 144-153.

[68] C. Cao, Q.H. Qin, A. Yu, Hybrid fundamental-solution-based FEM for piezoelectric materials, Computational Mechanics, 50(4) (2012) 397-412.

[69] C. Cao, A. Yu, Q.H. Qin, A new hybrid finite element approach for plane piezoelectricity with defects, Acta Mechanica, 224(1) (2013) 41-61.

[70] H. Wang, Q.H. Qin, Fracture analysis in plane piezoelectric media using hybrid finite element model, in: International Conference of fracture, 2013.

[71] Q.H. Qin, M. Lu, BEM for crack-inclusion problems of plane thermopiezoelectric solids, International Journal for Numerical Methods in Engineering, 48(7) (2000) 1071-1088.

[72] Q.H. Qin, Thermoelectroelastic solution for elliptic inclusions and application to crack–inclusion problems, Applied Mathematical Modelling, 25(1) (2000) 1-23.

[73] Q.H. Qin, Y.W. Mai, Crack growth prediction of an inclined crack in a half-plane thermopiezoelectric solid, Theoretical and Applied Fracture Mechanics, 26(3) (1997) 185-191.

[74] H.Y. Liu, Q.H. Qin, Y.W. Mai, Crack growth in composites with piezoelectric fibers, in: Proc. of the Third Int. Conf. for Mesomechanics, Xi'an, China, June 13-16, Tsinghua Univ. Press, Vol. 1, 2000, pp. 357-366.

[75] Q.H. Qin, Y.W. Mai, Multiple cracks in thermoelectroelastic bimaterials, Theoretical and Applied Fracture Mechanics, 29(2) (1998) 141-150.

[76] Q.H. Qin, Y.W. Mai, Thermal analysis for cracks near interfaces between piezoelectric materials, Localized Damage 1998: Fifth International Conference on Damage and Fracture Mechanics, (1998) 13-22.

[77] Q.H. Qin, S.W. Yu, An arbitrarily-oriented plane crack terminating at the interface between dissimilar piezoelectric materials, International Journal of Solids and Structures, 34(5) (1997) 581-590.

[78] Q.H. Qin, S.W. Yu, On the plane piezoelectric problem of a loaded crack terminating at a material interface, Acta Mechanica Solida Sinica, 9 (1996) 151-158.

[79] Q.H. Qin, Y.W. Mai, A closed crack tip model for interface cracks in thermopiezoelectric materials, International Journal of Solids and Structures, 36(16) (1999) 2463-2479.

[80] Q.H. Qin, Y.W. Mai, Crack path selection in piezoelectric bimaterials, Composite structures, 47(1) (1999) 519-524.

[81] Q.H. Qin, J.S. Wang, X. Li, Effect of elastic coating on fracture behaviour of piezoelectric fibre with a penny-shaped crack, Composite structures, 75(1) (2006) 465-471.

[82] J.S. Wang, Q.H. Qin, Penny-shaped Crack in a Solid Piezoelectric Cylinder With Two Typical Boundary Conditions, Journal of Beijing University of Technology, 32(S1) (2006) 29-34.

[83] Q.H. Qin, S. Yu, Logarithmic singularity at crack tips in piezoelectric media, Chinese science bulletin, 41(7) (1996) 563-566.

[84] W. Qiu, Y. Kang, Q. Sun, Q.H. Qin, Y. Lin, Stress analysis and geometrical configuration selection for multilayer piezoelectric displacement actuator, Acta Mechanica Solida Sinica, 17(4) (2004) 323-329.

[85] W. Qiu, Y.L. Kang, Q.H. Qin, Q. Sun, F. Xu, Study for multilayer piezoelectric composite structure as displacement actuator by Moire interferometry and

infrared thermography experiments, Materials Science and Engineering: A, 452 (2007) 228-234.

[86] J.S. Wang, Q.H. Qin, Symplectic model for piezoelectric wedges and its application in analysis of electroelastic singularities, Philosophical Magazine, 87(2) (2007) 225-251.

[87] C.-Y. Lee, Q.H. Qin, G. Walpole, Numerical modeling on electric response of fibre-orientation of composites with piezoelectricity, International Journal of Research and Reviews in Applied Science, 16(3) (2013) 377-386.

[88] Q.S. Yang, Q.H. Qin, T. Liu, Interlayer stress in laminate beam of piezoelectric and elastic materials, Composite structures, 75(1) (2006) 587-592.

[89] Q.S. Yang, Q.H. Qin, L. Ma, X. Lu, C. Cui, A theoretical model and finite element formulation for coupled thermo-electro-chemo-mechanical media, Mechanics of Materials, 42(2) (2010) 148-156.

[90] S.W. Yu, Q.H. Qin, Damage analysis of thermopiezoelectric properties: Part I—crack tip singularities, Theoretical and Applied Fracture Mechanics, 25(3) (1996) 263-277.

[91] S.W. Yu, Q.H. Qin, Damage analysis of thermopiezoelectric properties: Part II. Effective crack model, Theoretical and Applied Fracture Mechanics, 25(3) (1996) 279-288.

[92] K.S. Havner, A discrete model for the prediction of subsequent yield surfaces in polycrystalline plasticity, International Journal of Solids and Structures, 7(7) (1971) 719-730.

[93] H. Berger, S. Kari, U. Gabbert, R. Rodriguez-Ramos, R. Guinovart, J.A. Otero, J. Bravo-Castillero, An analytical and numerical approach for calculating effective material coefficients of piezoelectric fiber composites, International Journal of Solids and Structures, 42(21) (2005) 5692-5714.

[94] H. Wang, Q.H. Qin, Fundamental-solution-based hybrid FEM for plane elasticity with special elements, Computational Mechanics, 48(5) (2011) 515-528.

[95] H. Wang, Q.H. Qin, Fundamental-solution-based finite element model for plane orthotropic elastic bodies, European Journal of Mechanics-A/Solids, 29(5) (2010) 801-809.

[96] M. Dhanasekar, J. Han, Q.H. Qin, A hybrid-Trefftz element containing an elliptic hole, Finite Elements in Analysis and Design, 42(14) (2006) 1314-1323.

[97] Q.H. Qin, C.X. Mao, Coupled torsional-flexural vibration of shaft systems in mechanical engineering—I. Finite element model, Computers & Structures, 58(4) (1996) 835-843.

[98] Q.H. Qin, Hybrid Trefftz finite-element approach for plate bending on an elastic foundation, Applied Mathematical Modelling, 18(6) (1994) 334-339.

[99] Q.H. Qin, The Trefftz finite and boundary element method, WIT Press, Southampton, 2000.

[100] Q.H. Qin, Trefftz finite element method and its applications, Applied Mechanics Reviews, 58(5) (2005) 316-337.

[101] Q.H. Qin, Hybrid-Trefftz finite element method for Reissner plates on an elastic foundation, Computer Methods in Applied Mechanics and Engineering, 122(3-4) (1995) 379-392.

[102] H. Wang, Q.H. Qin, Hybrid FEM with fundamental solutions as trial functions for heat conduction simulation, Acta Mechanica Solida Sinica, 22(5) (2009) 487-498.

[103] Q.H. Qin, H. Wang, Matlab and C programming for Trefftz finite element methods, New York: CRC Press, 2008.

[104] J. Jirousek, Q.H. Qin, Application of hybrid-Trefftz element approach to transient heat conduction analysis, Computers & Structures, 58(1) (1996) 195-201.

[105] Q.H. Qin, X.Q. He, Variational principles, FE and MPT for analysis of non-linear impact-contact problems, Computer methods in applied mechanics and engineering, 122(3) (1995) 205-222.